small NANO MICRO

Molecular junctions

DOI: 10.1002/smll.200701232

High-Fidelity Formation of a Molecular-Junction Device Using a Thickness-Controlled Bilayer Architecture

*Gyeong Sook Bang, Hojong Chang, Ja-Ryong Koo, Takhee Lee, Rigoberto C. Advincula, and Hyoyoung Lee**

The device yield of molecular junctions has become a major issue for the practical application of molecular electronics based on a crossbar system of a metal–molecule–metal (MMM) junction. As the thickness of self-assembled monolayers (SAMs) is typically 1–2 nm, it is difficult to avoid electrical shorts due to the penetration of top metal particles into the SAMs. A simple and effective strategy for the creation of a reliable molecular junction using a thickness-controlled bilayer with a bifunctional heterostructure is presented. In the MMM device, the Au adlayer on the molecular layer is spontaneously formed with deposition of the top Au metals and the sandwiched molecular layer maintains the quality of the SAMs. This method greatly reduces electrical shorts by preventing the diffusion of the top metal electrode and offsetting the surface roughness of the bottom metal electrode, resulting in a device yield of more than 90%.

Keywords:
- bilayers
- molecular electronics
- molecular junctions
- monolayers
- self-assembly

1. Introduction

The prospect of molecular electronics based on a crossbar system of a metal–molecule–metal (MMM) junction is driven by the implementation of integrated circuits above the terabit level, where self-assembled monolayers (SAMs) capable of highly integrated density are used as active switching components. Organic SAMs have been intensively studied as a powerful means of surface modification and functionalization with molecular-level control. They have proven to be useful models for molecular-electronic devices.[1–3] Some organic molecules with appropriate electronic properties can be used for rectification,[4–7] negative differential resistance,[8] and conductance switching.[9–12] However, the use of SAMs for MMM devices has been limited due to the low device yield of approximately 1.5–5%, which is mainly attributed to electrical shorting.[13,14] To reduce the degree of electrical shorting, issues such as the compactness and robustness of the SAMs, the use of an additive layer on the SAMs, a nanometer-sized surface area of the metal electrode, and surface roughness of the metal electrode have all been considered.[3,7,15,16] In the case of a nanometer-sized electrode, Zhou et al. used ''nano via holes'', nanometer holes formed in the SiN_x insulating layer by reactive-ion etching to expose the nanometer-sized area of the Au bottom electrode. They reported that a smaller diameter of the nano via hole provides a higher yield by reducing the size of the potential defect area.[7] Nevertheless, some researchers have reported a low and fluctuating yield in a practical crossbar-type molecular device using alkylthiol SAMs in nanopore (100-nm diameter) patterns.[17] It is, therefore, difficult to avoid electrical shorts due to the penetration of top metal particles into the SAMs because the thickness of the SAMs is typically 1–2 nm. To address the

[*] Dr. G. S. Bang, H. Chang, Dr. J.-R. Koo, Dr. H. Lee
National Creative Research Initiative
Center for Smart Molecular Memory
IT Convergence & Components Laboratory
Electronics and Telecommunications Research Institute (ETRI)
161 Gajeong-dong, Yuseong-gu, Daejeon 305–350 (South Korea)
E-mail: hyoyoung@etri.re.kr

Prof. T. Lee
Heeger Center for Advanced Materials
Department of Materials Science and Engineering
Gwangju Institute of Science and Technology
Gwangju 500–712 (South Korea)

Prof. R. C. Advincula
Department of Chemistry
Department of Chemical Engineering
University of Houston
Houston, TX 77204 (USA)

Supporting Information is available on the WWW under http://www.small-journal.com or from the author.

reduction of electrical shorts of the SAMs, thickness-controlled and self-assembled bifunctional molecular layers formed in situ were introduced for the fabrication of a crossbar-array molecular junction using a nano via hole with a diameter of 170 nm. The nano via hole is a useful structure for testing a number of devices in crossbar-type molecular electronics. Organic SAMs with alkyl chains longer than ten units have been reported to be very good insulators.[18] Therefore, they can be applied to the fabrication of an insulator–conductor structure for a molecular-junction device. In a previous report,[19] the authors introduced an 11-amino-1-undecanethiol (AUT) bilayer of an alkanethiol bifunctional molecule with a height of 3.5 nm and a rose bengal (RB) functional group with a molecular memory effect on the AUT bilayer (RB–TUA–AUT). It was demonstrated that the RB–TUA–AUT film consisted of a highly ordered structure and acted as an effective blocking layer.

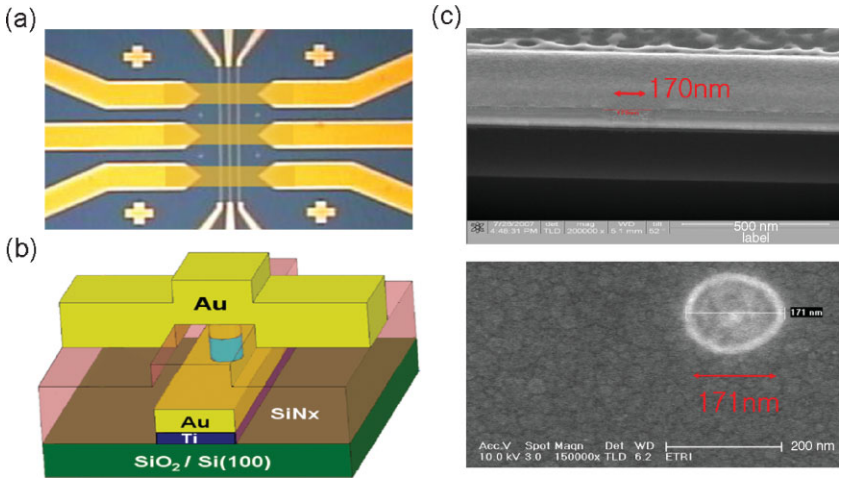

Figure 1. a) Photograph of a 3 × 3-array-patterned chip device including 9 nano via holes. b) Schematic diagram of the nano via hole device. c) Focused ion beam (top) and SEM (bottom) images of a 170-nm nano via hole.

This study reports the fabrication of nanoscale crossbar-array devices, the characterization of the interaction between the top Au metals and the RB-bilayered SAM, and the application of an RB-bilayered SAM in nanoscale crossbar-array devices. A simple and effective strategy for reliable molecular junctions using a thickness-controlled bilayer with a bifunctional heterostructure is introduced. The yield of the molecular junction devices is shown to be greater than 90% using RB-bilayered SAMs of bifunctional heterostructures with free thiol-terminated bilayer SAMs. This is shown to be a breakthrough that allows a reduction of the effect of the surface roughness of the bottom electrode. Moreover, it prevents the penetration of the top electrode. This is the first known report that addresses offsetting the surface roughness of bottom metal electrodes mainly by increasing the film thickness with RB-bilayered SAMs.

2. Results and Discussion

2.1. Fabrication of the Au–Organic SAMs–Au Molecular MMM Junction Device

A nano via hole device with a diameter of 170 nm and a large enough area for a feasibility test in molecular electronics was fabricated by electron-beam lithography and magnetically enhanced reactive-ion etching (MERIE; see Supporting Information, Figure S1, for further details regarding the fabrication process). Figure 1a–c shows a photograph of the chip device, a schematic diagram of the MMM junction device, and a focused-ion beam and scanning electron microscopy (SEM) image of the 170-nm nano via hole. The fabricated chip contains nine individual junctions (Figure 1a). To investigate the effect of offsetting the surface roughness of the bottom Au electrode using a bilayer in the nano via hole, Au film test samples were prepared under the same conditions as the Au bottom electrode of the nano via hole device. This can be obtained with a straightforward preparation and applied to an actual product. The root-mean-square (rms) surface roughness of the Au film, as measured by atomic force microscopy (AFM), was nearly 1.4 nm over a scan area of 1 μm^2 (see Supporting Information, Figure S2). As was previously reported,[19] the organic bilayer (TUA–AUT) was prepared together on the Au film and the bottom Au electrode of the nano via hole by a self-assembly method. The RB molecule was then introduced on to the thiol-terminated bilayer to result in an RB–TUA–AUT film. The AFM images of TUA–AUT and RB–TUA–AUT films show reduced surface roughness with rms values of 0.35 nm for the TUA–AUT film and 0.42 nm for the RB–TUA–AUT film (see Supporting

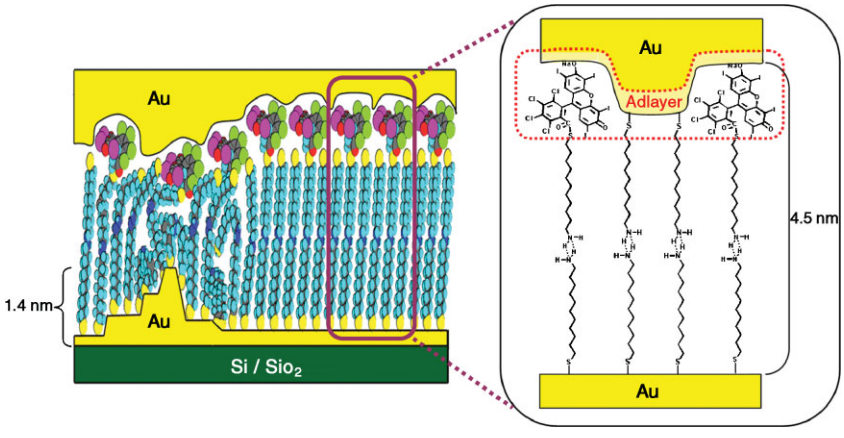

Figure 2. Schematic diagram of the RB–TUA–AUT layer (4.5-nm thickness) sandwiched between the bottom Au electrode of the nano via hole (1.4 nm, rms) and the top Au electrode.

small NANO MICRO

Information, Figure S2). The device structure of the RB–TUA–AUT film is depicted in Figure 2. Finally, Au metal for the top electrode was vapor deposited onto organic SAMs using an electron-beam vacuum evaporator under a low temperature (≈140–160 K) and low deposition rate (≈0.2 Å s^{-1}) in order to avoid thermal damage to the organic layer. It is known that one of the major drawbacks when the top metal electrode is deposited is the penetration of metal particles into the SAMs. This causes the stability of organic SAMs to deteriorate, resulting in a very low yield.[14,17] Furthermore, in the molecular structure shown in Figure 2, it is expected that, when the top Au metal is deposited, the unreacted thiol group of the TUA–AUT plays an important role in forming the adlayer, which may prevent the penetration of metal particles.

To verify the nano via hole device, the current–voltage (*I–V*) characteristics were measured using a semiconductor parameter analyzer. The *I–V* characteristics of a crossbar junction without a nano via hole exhibited a negligible amount of leakage current (≈10 fA at 2 V bias), demonstrating the insulating layer of the SiN_x. The *I–V* characteristics of a crossbar junction with an open nano via hole (with no SAM) showed expected ohmic behavior of a short (≈20 mA at 2 V bias), proving the existence of exposed Au in the nano via hole.

2.2. Characterization of the Au–Organic SAMs and the Au–Organic SAMs–Au Molecular Junction

2.2.1. Formation of the Adlayer Between the Top Electrode and the RB-Bilayered SAMs

The formation of the molecular layer was confirmed using a spectroscopic ellipsometer and X-ray photoelectron spectroscopy (XPS; see Supporting Information, Figure S3, for the spectra of spectroscopy ellipsometer and Figure S4 for the XPS analysis of RB–TUA–AUT film on Au). The thicknesses of the TUA–AUT film and the RB–TUA–AUT film were approximately 3.5 nm and 4.5 nm, respectively. The refractive index values of these films were between 1.4 and 1.8, respectively, in a wavelength range of 200–850 nm. The absorption band near 560 nm in the extinction curve of the RB–TUA–AUT film was attributed to the maximum electronic transition of the RB. The surface coverage of the TUA–AUT by quartz crystal microbalance (QCM) data is 4.2×10^{18} molecules m^{-2}. The RB coverage on RB–TUA–AUT was estimated through a comparison of sulfur and iodine quantification in the XPS data (see Supporting Information for more details). The RB coverage on the RB–TUA–AUT is 1.1×10^{18} molecules m^{-2}, which corresponds to a single monolayer. The ratio of the coverage values for RB and TUA–AUT was 1:3.8 RB/TUA–AUT in RB–TUA–AUT. It can be estimated that approximately one quarter of the TUA–AUT reacts with RB.

In order to confirm the evaporation effect of top Au on the RB-bilayered SAMs, the interface structure between the top electrode and the RB–TUA–AUT surface was investigated by XPS and Fourier transform infrared (FTIR) analyses before and after the vapor deposition of the top Au metal (1.5-nm thickness). First, the XPS spectra of the RB–TUA–AUT film in the S 2p and Au 4f regions, before and after the deposition of Au, were observed with different takeoff angles of 30° and 90°. At a takeoff angle of 30°, the effective sampling depths of the XPS are in the range of 4 to 5 nm.[20] The S 2p spectra taken at a 30° takeoff angle are shown in Figure 3a. Prior to the top Au deposition (the black line in Figure 3a), two components in the S 2p spectra were observed at 162.7 and 168.2 eV for bound sulfur species on the bottom Au surface and oxidized sulfur species of the exposed terminal sulfur, respectively. This is in good agreement with previous studies of thiol-terminated SAMs.[19–22] After the top Au deposition, the peak intensity of the exposed terminal sulfur at 168.2 eV decreases dramatically and, instead, a broader peak (162.7 eV) appears due to the bonding with the top Au particles. As assumed, if Au forms an adlayer on the top of the thiol-terminated SAMs, the ratio of the peak area for S 2p (at 168.3 eV)/S 2p (at 162.7 eV) decreases as the deposition of the top Au metal proceeds. Essentially, the ratio without the top Au (0.69) decreased to the value of the top Au (0.35) metal. On the other hand, the S 2p peaks show no peak shift for the binding energy and the peak intensity scarcely changed even with different takeoff angles. Hence, it was confirmed that, as the interactions between the top Au metal and the free sulfurs on the thiol-terminated bilayer increase, the remaining free sulfur atoms

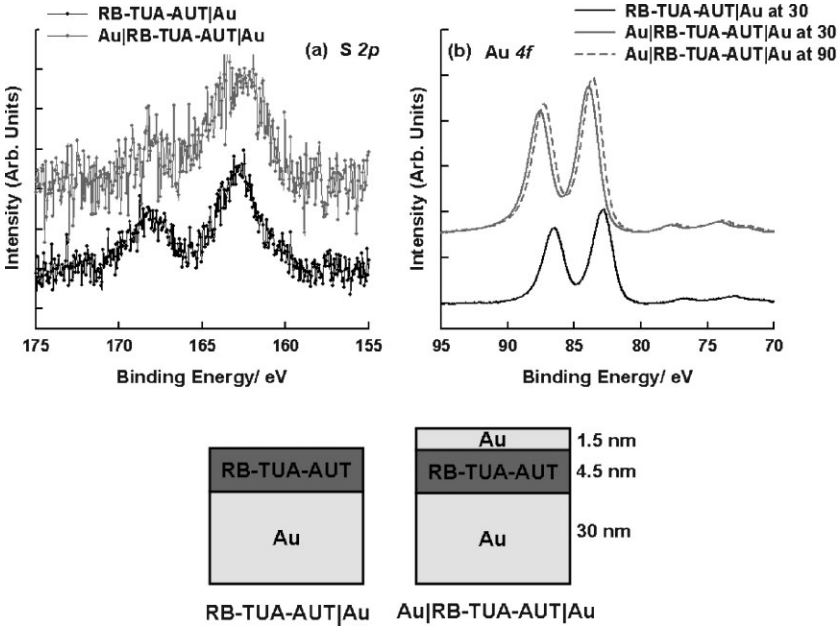

Figure 3. a) XPS spectra of S 2p of the RB–TUA–AUT film with and without the top Au metal electrode at a 30° takeoff angle. b) XPS spectra of Au 4f of the RB–TUA–AUT film before and after the top Au deposition at different takeoff angles. The Au 4f intensities of (b) are scaled to the identical values of the peak height for comparing the peak position and shape.

decrease along with the formation of the adlayer. Furthermore, the Au 4f core-level binding shift revealed the thickness effect of the organic film.[23] The Au 4f spectra taken at 30° and 90° takeoff angles are shown in Figure 3b. With the top Au deposition, the intensity of the Au 4f spectra taken at the 30° takeoff angle increases considerably and the binding energy shifts to a higher value. This shift toward a higher binding energy implies that the Au atoms form an adlayer on the RB-bilayered SAMs. These results from the S 2p and Au 4f spectra reflect the interaction of the Au atoms with the exposed thiol groups of the RB–TUA–AUT. Furthermore, in comparison of the Au 4f spectra of Au–RB–TUA–AUT–Au taken at different takeoff angles of 30° and 90°, the shift of the binding energy and the intensity appear to be independent of the takeoff angle in both cases.

In order to investigate the circumstance of the sulfur-containing functional groups by deposition of top metal, the chemical interaction of the top Au atoms on the SAMs was then cross characterized using an FTIR spectrophotometer. Vibrational spectroscopy is able to analyze organic films with a top metal coating of a few nanometers and represents the most attractive method of investigating structural and conformational analyses of molecules at interfaces. In actuality, IR studies of the deposition (1–3-nm thickness) of various top-metal atoms (including gold) on thiolate SAMs have been reported.[24,25] Therefore, this method makes it possible to probe the effect of the penetration and chemical interaction of metal atoms with SAMs. Figure 4 shows IR spectra for methylene stretches of the RB–TUA–AUT film before and after the top Au deposition. The methylene stretching region determines the characteristics of SAMs with alkyl chains for a close-packed and well-ordered film. Moreover, it is indicative of the direct changes in the interactions of the CH_2 groups caused by the top Au deposition. For the RB–TUA–AUT film without top Au metal, asymmetric (ν_{asym}) and symmetric (ν_{sym}) methylene stretches were observed at 2923 and 2850 cm^{-1}, respectively. After the deposition of 1.5 nm of Au on top of the RB–TUA–AUT film, the spectra showed little change (2922 and 2851 cm^{-1}) in the C–H stretching region. The full width at half-maximum (fwhm) of the ν_{asym} (CH_2) peak was determined to be 36.0 cm^{-1} and 36.4 cm^{-1}

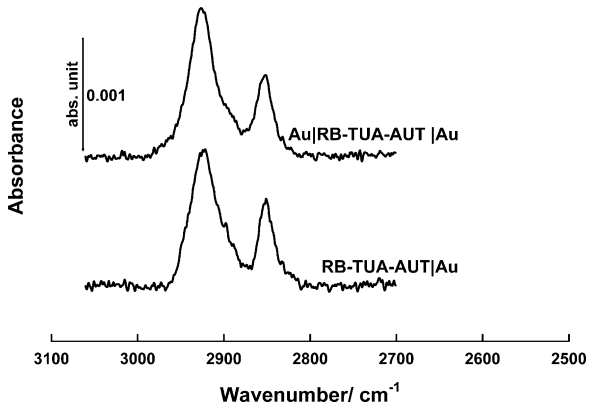

Figure 4. The $-CH_2$ stretching vibration peaks of grazing angle FT-IR spectra of the RB–TUA–AUT film with (upper) and without (bottom) the top Au metal layer (1.5 nm).

before and after the top Au deposition, respectively. The top Au deposition appears to result in little broadening of the C–H stretch and in less interaction of the top Au atoms with the alkyl groups. This indicates that the degree of perturbation of the RB–TUA–AUT film under top Au deposition is very low. These results also support the notion that the top Au metal does not penetrate into the RB–TUA–AUT film but, rather, helps to form the adlayer on the RB–TUA–AUT film. These experiments were repeated four times and reproducible results were obtained. In a previous report by the authors,[19] it was also demonstrated that the RB–TUA–AUT film consisted of a highly ordered structure and acted as an effective blocking layer, as confirmed via grazing-angle FTIR spectroscopy and cyclic voltammetry (CV).

These results indicate that top Au evaporation does not destroy RB-bilayered SAMs that include sulfur-containing functional groups. It can be expected that the RB–TUA–AUT film effectively blocks the diffusion of the Au metal and helps overcome the electrical shorting problems, resulting in a high yield.

2.2.2. Current-Density–Voltage (J–V) Characteristics of the Molecular MMM Junction Device

In order to apply the RB-bilayer SAMs in crossbar-type molecular electronics, the current-density–voltage (J–V) characteristics of the Au–organic SAMs–Au molecular-junction device were examined. The J–V characteristics of the TUA–AUT device used as a control and the RB–TUA–AUT device with a nano via hole are shown in Figure 5. The sweeping bias voltage was repeatedly cycled from -1 V to $+1$ V to -1 V. The J–V curves of the TUA–AUT device are fairly symmetric at approximately $V = 0$, as illustrated by inverting and superposing negative bias. The J–V characteristics of the RB–TUA–AUT device show symmetric and hysteretic properties. The RB molecule has acceptor groups that induce partial nonconjugation in the molecular backbone. It has been reported that an RB molecule in the structure of an ITO–RB monolayer–Hg device[26,27] switches to a high-conducting state due to electroreduction under an applied bias voltage. Compared with the J–V characteristic of the TUA–AUT device, it can be demonstrated that the RB is the origin of the hysteresis in the RB–TUA–AUT device.[19]

The current density of the TUA–AUT (5.91 A cm^{-2} at 0.1 V) and the RB–TUA–AUT (1.78 A cm^{-2} at 0.1 V) devices showed significantly lower values compared to the reported alkanedithiol SAM device[16,18] ($1.5 \pm 0.2 \times 10^3$ A cm^{-2} at 1.0 V) in the MMM structure. In particular, the value of the RB–TUA–AUT device is lower than that of the TUA–AUT device. The junction resistivity of the proposed devices (Figure 5, inset) was calculated using the linear least-squares fit of the J–V curves between -0.5 V and $+0.5$ V. The average junction resistivity was 2373 GΩ nm^2 for the TUA–AUT device and 3910 GΩ nm^2 for the RB–TUA–AUT device. These values were over two orders of magnitude greater compared to the reported data of an AFM measurement of the heptanethiol (HT, 10 GΩ nm^2).[28,29] This discrepancy can be attributed to the longer molecular length of the bilayer.

NANO MICRO small

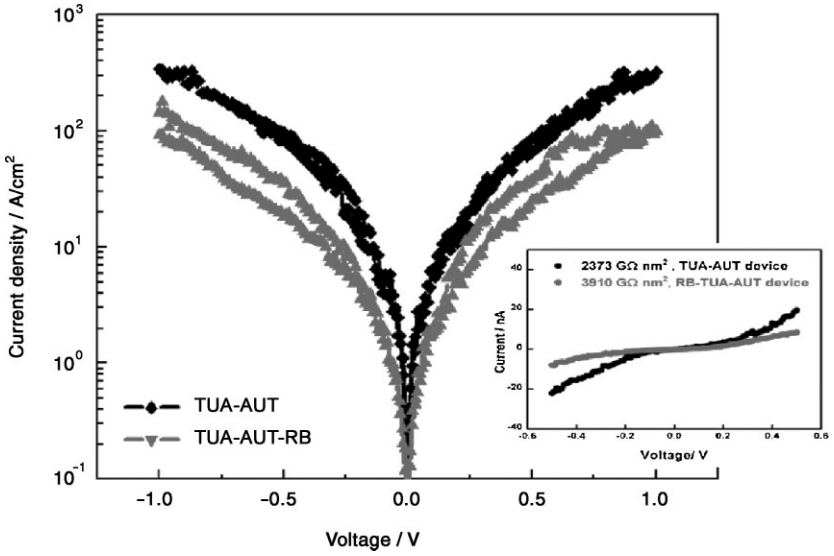

Figure 5. Current density–voltage (*J-V*) characteristics in semi-log scale and normalized *I-V* curves between −0.5 V and +0.5 V (inset) for the TUA–AUT device (black line) and the RB–TUA–AUT device (grey line) in the nano via hole with a 170-nm diameter.

As expected, the RB–TUA–AUT junction with a longer molecular length shows good bifunctional insulator behavior.

2.2.3. Relationship Between Device Yield and the Molecular Length in the Molecular MMM Junction

As mentioned earlier, most crossbar junctions in the vertical structure of MMM devices are electrically shorted.[30] This often occurs when depositing metal on the top of a simple alkanethiol single monolayer such as a 1-dodecanethiol (DT). In the present case, all DT devices with nano via holes were electrically shorted. To understand the effective offsetting length, an RB–DDT device was prepared using an RB monolayer on a 1,12-dodecanedithiol (DDT) monolayer, which has a structure that is similar to that of the RB–TUA–AUT device except for the molecular length. The molecular length of the RB-DDT is approximately 2.9 nm while the molecular length of the DDT (1.9 nm) is approximately half that of the TUA–AUT (3.5 nm). The yield of the RB-DDT device was nearly 0–1%. From these results, it can be concluded that the length of the DDT or the RB-DDT cannot sufficiently maintain the quality of the SAM layer for the surface roughness of the Au bottom electrode (1.4 nm, rms). On the other hand, the yield of the TUA–AUT device is 11% in the nano via hole, which is considerably higher than the yields of the alkanethiol monolayer devices (≈1.5–5%) and higher than the control experiments involving DT (0%) and RB–DDT (0–1%). Remarkably, the yield of the RB–TUA–AUT device in the nano via hole is 94% (102 out of 108) and the reproducibility of the hysteretic *J–V* curve is high (see Supporting Information, Figure S5, regarding the reproducible *J–V* characteristics of RB–TUA–AUT devices). The RB–TUA–AUT device showed stable behavior between +1 V and −1 V for a few cycles. From these results, it can be concluded that the device yield is directly related to the molecular length in terms of offsetting the surface roughness of the bottom metal electrode. Although the distance between the two Au layers was increased by introducing the bilayer in the proposed device, the maximum length of the molecular bilayer is 3.5–4.5 nm, which is very thin nonetheless. The operating voltage of the RB-bilayer device is within ±1 V.

3. Conclusions

A nanoscale molecular device with a vertical MMM structure, along with a novel method to improve the device yield sharply via the simple preparation and the use of thickness-controlled bifunctional bilayers, is demonstrated in this study. With the help of the bifunctional heterostructure, which strongly blocks penetration of the top metal, the device yield is higher than 90%.

This is the first known achievement of its kind that reduces the effect of the intrinsic surface roughness of the bottom metal electrode on device performance. The results of this study show that a bifunctional heterostructure with a film thickness of ≈4–5 nm can be an effective means of regulating the generation of electrical shorts in the crossbar systems of molecular electronics devices. The proposed technique offers the advantages of a simple approach and potentially lower fabrication costs for molecular electronics.

4. Experimental Section

Device fabrication: The device fabrication began with a p-type Si(100) wafer covered with thermally grown SiO_2 to a thickness of 300 nm. Patterned bottom electrodes with a Ti(5 nm)/Au(30 nm) stacking structure were prepared via electron-beam vacuum techniques, fabricated in a normal photolithography method, and then deposited with a SiN_x layer at a thickness of 60 nm using plasma-enhanced chemical vapor deposition (PECVD). A nano via hole with a diameter of 170 nm was formed through the SiN_x layer by MERIE in C_2F_6.

Preparation of Au–organic SAM–Au device: First, the bottom Au electrodes of the nano via hole and the Au film test samples were cleaned using piranha solution (98% H_2SO_4: 30% H_2O_2 = 3:1, v/v) for 3 min. This was followed by washing several times with deionized water and ethanol and finally drying with a stream of nitrogen gas. *Caution: piranha solution reacts violently with most organic materials and should be handled with extreme care*. As in a previously reported method,[19] the TUA–AUT films on the cleaned bottom Au electrode and the Au film test

samples were prepared by soaking them in a solution containing 3 mM AUT in dimethylformamide (DMF) for 24 h. For the formation of the RB layer on the TUA–AUT, the prepared TUA–AUT film was introduced to a solution containing 0.5 mM RB and 10 mM 1-ethyl-3-(3-dimethylaminopropyl) carbodiimide hydrochloride (EDC) in ethanol and it was reacted by shaking for 15 h to obtain the RB–TUA–AUT layer. The modified gold bottom electrodes and Au film test samples were rinsed thoroughly with DMF and ethanol and were then dried with a stream of nitrogen gas. These bottom electrodes and test samples were immediately transferred to an electron-beam vacuum evaporator. Before the evaporation of the top Au metal, the modified electrodes and test samples with the organic molecules were kept in a chamber at a temperature ranging from 140–160 K under a pressure of 5×10^{-7} Torr for 6 h. A patterned top Au electrode with a thickness of 70 nm (or 1.5 nm) was deposited through a shadow mask onto molecular layers using the electron-beam vacuum evaporator. The evaporation process was also continuously monitored with a quartz-crystal thickness monitor. The evaporation rate of the top Au metal was maintained at 0.2 Å s^{-1} under 5×10^{-7} Torr and the temperature of the substrate-loading samples was held constant at 140 K to avoid possible damage to the molecular layer by direct heat from the evaporation source.

Measurements: The nano via hole was characterized using a scanning electron microscope (SIRION series, FEI Company) operating at a beam voltage of 10 kV and by a focused ion beam instrument (FIB, NOVA 200, FEI Company).

For the characterization of the surfaces of the Au–organic SAMs (without top metal) and the Au–organic SAMs–Au (with top metal of 1.5-nm thickness) using AFM, a spectroscopic ellipsometer, grazing-angle FTIR, and XPS, the Au film test samples were prepared under conditions that were identical to those of the Au bottom electrode of the nano via hole device. Ellipsometric spectra for the TUA–AUT and the RB–TUA–AUT films were taken using a spectroscopic ellipsometer (Model J.A. Woollam VASE.) at an incident angle of 60° to 70° in a wavelength range between 200 and 850 nm. The thickness and optical constants of the films can be determined from the measured ellipsometric parameters. The surface morphology of the TUA–AUT and the RB–TUA–AUT films were determined by imaging with a multimode Nanoscope IV (Digital Instrument) AFM. FTIR spectra were obtained in single-reflection mode using a dry N_2-purged Thermo Nicolet Nexus grazing-angle FTIR equipped with the SAGA (smart aperture grazing angle) accessory. All spectra were obtained at a resolution of 2 cm^{-1} with 2000 scans. XPS spectra were obtained using a VG Scientific ESCA-200R X-ray photoelectron spectrometer with an Al Kα source. The pressure of the analysis chamber remained below 1×10^{-9} Torr. A pass energy of 50 eV, an energy step of 0.05 eV, and an X-ray power of 250 W were used in the analysis. The binding energy with a bulk Au 4f level at 84.0 eV was used as a reference. Spectra were taken at photoelectron takeoff angles of 30° and 90° between the electrode surface and the direction of the photoelectrons detected by the analyzer. The spectra were acquired from Au–organic SAMs (without top metal deposition) and Au–organic SAMs–Au (with top metal deposition) surfaces. For a better comparison of the Au 4f and S 2p peaks, all spectra were normalized with baseline correction. *I–V* measurements of the nano via hole MMM device were performed in an enclosed shield box using a Keithley 4200 Semiconductor Characterization System Unit at room temperature. The voltage was initially swept from 0 V to 1.0 V at an interval of 10 mV every 100 ms to the bottom electrode and was subsequently applied from 1.0 V to −1.0 V to 0 V in voltage loops.

Acknowledgements

This work was supported by the Creative Research Initiatives (project title: Smart Molecular Memory) of MOST/KOSEF. We thank Professor J. S. Lindsey of the Chemistry Department, North Carolina State University for many valuable conversations on the molecular-junction device. We also thank Dr. Yong-jai Cho of the Korea Research Institute of Standard and Science (KRISS) and Dr. Jonghyurk Park of Electronics and Telecommunications Research Institute (ETRI) for spectroscopic ellipsometer and XPS analyses.

[1] D. K. Aswal, S. Lenfant, D. Guerin, J. V. Yakhmi, *Anal. Chim. Acta* **2006**, *568*, 84.
[2] R. L. Carroll, C. B. Gorman, *Angew. Chem. Int. Ed.* **2002**, *41*, 4378.
[3] J. Christopher Love, L. A. Estroff, J. K. Kriebel, R. G. Nuzzo, G. M. Whiesides, *Chem. Rev.* **2005**, *105*, 1103.
[4] G. J. Ashwell, J. R. Sambles, A. S. Martin, W. G. Parker, M. Szablewski, *J. Chem. Soc. Chem. Commun.* **1990**, *19*, 1374.
[5] R. M. Metzger, *Chem. Rev.* **2003**, *103*, 3803.
[6] E. E. Polymeropoulos, J. Sagiv, *J. Chem. Phys.* **1978**, *69*, 1836.
[7] C. Zhou, M. R. Deshpande, M. A. Reed, L. Jones, J. M. Tour, *Appl. Phys. Lett.* **1997**, *71*, 611.
[8] A. S. Martin, J. R. Sambles, G. J. Ashwell, *Phys. Rev. Lett.* **1993**, *70*, 218.
[9] J. Chen, M. A. Reed, A. M. Rawlett, J. M. Tour, *Science* **1999**, *286*, 1550.
[10] Z. J. Donhauser, B. A. Mantooth, K. F. Kelly, L. A. Bumm, J. D. Monnell, J. J. Stapleton, J. D. W. Price, A. M. Rawlett, D. L. Allara, J. M. Tour, P. S. Weiss, *Science* **2001**, *292*, 2303.
[11] C. N. Lau, D. R. Stewart, R. S. Williams, M. Bockrath, *Nano Lett.* **2004**, *4*, 569.
[12] Z. Liu, A. A. Yasseri, J. S. Lindsey, D. F. Bocian, *Science* **2003**, *302*, 1543.
[13] M. D. Austin, S. Y. Chou, *Nano Lett.* **2003**, *3*, 1687.
[14] T. Kim, G. Wang, H. Lee, T. Lee, *Nanotechnology* **2007**, *18*, 315204.
[15] H. B. Akkerman, P. W. M. Blom, D. M. de Leeuw, B. de Boer, *Nature* **2006**, *441*, 69.
[16] W. Wang, T. Lee, M. A. Reed, *Phys. Rev. B* **2003**, *68*, 035416.
[17] J. Deng, W. Hofbauer, N. Chandrasekhar, S. J. O'Shea, *Nanotechnology* **2007**, *18*, 155202.
[18] T. Lee, W. Wang, J. F. Klemic, J. J. Zhang, J. Su, M. A. Reed, *J. Phys. Chem. B* **2004**, *108*, 8742.
[19] G. S. Bang, J. Park, J. Lee, N.-J. Choi, H.-Y. Baek, H. Lee, *Langmuir* **2007**, *23*, 5195.
[20] J. F. Watts, J. Wolstenholme, *An Introduction to Surface Analysis by XPS and AES*, Wiley, UK **2003**.
[21] S. R. Johnson, S. D. Evans, R. Brydson, *Langmuir* **1998**, *14*, 6639.
[22] D. V. Leff, L. Brandt, J. R. Heath, *Langmuir* **1996**, *12*, 4723.
[23] T. Ohji, H.-Y. Sheng, Z.-C. Dong, H. Nejoh, D. Fujita, *Appl. Phys. Lett.* **2001**, *79*, 2453.

[24] B. de Boer, M. M. Frank, Y. J. Chabal, W. Jiang, E. Garfunkel, Z. Bao, *Langmuir* **2004**, *20*, 1539.
[25] A. V. Walker, T. B. Tighe, O. M. Cabarcos, M. D. Reinard, B. C. Haynie, S. Uppili, N. Winograd, D. L. Allara, *J. Am. Chem. Soc.* **2004**, *126*, 3954.
[26] A. Bandyopadhyay, A. J. Pal, *Appl. Phys. Lett.* **2003**, *82*, 1215.
[27] S. K. Majee, A. Bandyopadhyay, A. J. Pal, *Chem. Phys. Lett.* **2004**, *399*, 284.
[28] N. Gosvami, K. H. A. Lau, S. K. Sinha, S. J. O'Shea, *Appl. Surf. Sci.* **2006**, *252*, 3956.
[29] D. J. Wold, C. D. Frisbie, *J. Am. Chem. Soc.* **2001**, *123*, 5549.
[30] Z. Zhu, T. A. Daniel, M. Maitani, O. M. Cabarcos, D. L. Allara, N. Winograd, *J. Am. Chem. Soc.* **2006**, *128*, 13710.

Received: December 10, 2007
Revised: May 21, 2008

